# Malaysian Journal of Analytical Sciences (MJAS)



Published by Malaysian Analytical Sciences Society

### In Silico MODELLING OF DRUG ADSORPTION USING AMINE-FUNCTIONALIZED IRMOF-74-III METAL-ORGANIC FRAMEWORKS

(Pemodelan Penjerapan Ubat menggunakan Rangkaian Logam-Organik IRMOF-74-III Terfungsi-Amina Secara *In Silico*)

Mostafa Yousefzadeh Borzehandani<sup>1,2</sup>, Emilia Abdulmalek<sup>1,2</sup>, Mohd Basyaruddin Abdul Rahman<sup>1,2,4</sup>, and Muhammad Alif Mohammad Latif<sup>1,3,4\*</sup>

<sup>1</sup>Integrated Chemical BioPhysics Research,
Faculty of Science,
Universiti Putra Malaysia, 43400 UPM Serdang, Selangor, Malaysia
<sup>2</sup>School Department of Chemistry,
Faculty of Science,
Universiti Putra Malaysia, 43400 UPM Serdang, Selangor, Malaysia
<sup>3</sup>Centre of Foundation Studies for Agricultural Science,
Universiti Putra Malaysia, 43400 UPM Serdang, Selangor, Malaysia
<sup>4</sup>Institute of Nanoscience and Nanotechnology,
Universiti Putra Malaysia, 43400 UPM Serdang, Selangor, Malaysia

\*Corresponding author: aliflatif@upm.edu.my

Received: 21 September 2022; Accepted: 30 January 2023; Published: 22 February 2023

#### Abstract

Metal-organic frameworks (MOFs) have been touted as prospective materials for drug storage and delivery. Functionalizing MOFs with an amine group has proven to be a successful strategy to achieve enhanced drug adsorption. To the best of our knowledge, however, there no report has been published showing the impact of increasing a common functional group such as amine on MOF's performance for drug adsorption. With the aim of exploring this possibility, IRMOF-74-III (IRM3) was functionalized with the amine group in various numbers and positions on the phenyl ring of the organic linker. The ability to adsorb several candidate drugs, including aspirin (Asp), fenbufen (Fen), ibuprofen (Ibu) and naproxen (Nap), were tested using density functional theory calculations and molecular docking. When the number of the amines increased, the MOF's pore polar surface area increased, but the energy gap between the HOMO and LUMO orbitals was reduced. Different pockets on the amine-functionalized IRM3's pore wall were analyzed by electrostatic potential contours, and then further investigated by a docking simulation. Fen@MOF was shown to be the most stable drug@MOF complex system, as demonstrated by the highest binding affinity. Coordinatively unsaturated magnesium sites in the frameworks, as well as hydroxyl and carbonyl groups on the drugs, are crucial for the interactions and charge transfer. This work successfully highlighted that having different numbers and positions of the amine group on the organic linker can affect the drug adsorption behavior of IRM3 MOF.

**Keywords:** amine-functionalized, anti-inflammatory drug adsorption, IRMOF-74-III, metal-organic frameworks, molecular docking

#### Abstrak

Rangkaian logam-organik (MOF) telah diketengahkan sebagai bahan prospektif bagi penyimpanan dan penghantaran ubatan. Berkenaan ini, memfungsikan MOFs dengan kumpulan amina adalah strategi yang berjaya bagi menambah baik jerapan ubatan. Walaubagaimanapun, mengikut pengetahuan kami, buat masa kini masih tiada laporan menunjukkan impak penambahan kumpulan berfungsi umum seperti amina terhadap prestasi MOF bagi jerapan ubatan. Dengan tujuan menerokai kemungkinan ini, IRMOF-74-III (IRM3) telah difungsikan dengan kumpulan amina dengan jumlah dan kedudukan yang berbeza pada cincin fenil penyambung organik. Kemampuan untuk menjerap beberapa calon ubat termasuklah aspirin (Asp), fenbufen (Fen), ibuprofen (Ibu) dan naproxen (Nap) telah diuji menggunakan pengiraan teori berfungsi ketumpatan dan pendokkan molekul. Adalah didapati bahawa jika jumlah kumpulan amina meningkat, permukaan berkutub MOF juga meningkat tetapi jurang tenaga di antara orbital HOMO dan LUMO adalah berkurang. Saku berbeza pada dinding rongga IRM3 terfungsi-amina dianalisa menggunakan kontur keupayaan elektrostatik dan disiasat lebih lanjut oleh simulasi pendokkan. Fen@MOF mempamerkan sistem kompleks drug@MOF yang paling stabil dan disahihkan oleh afiniti pengikat tertinggi. Tapak magnesium tak tepu yang terselaras di dalam rangkaian, dan juga kumpulan hidroksil dan karbonil pada ubat adalah penting bagi saling tindakan dan pemindahan cas. Kerja ini berjaya mengetengahkan yang memiliki kumpulan amina pada jumlah dan posisi berbeza pada penyambung organik boleh memberi kesan kepada sifat penjerapan ubatan MOF IRM3.

Kata kunci: terfungsi-amina, penjerapan ubat anti-inflamasi, IRMOF-74-III, rangka logam-organik, pendokkan molekul

#### Introduction

Metal-organic frameworks (MOFs) are a class of porous materials constructed by a mixture of metal nodes and organic linkers [1]. They have been extensively investigated in numerous applications, such as catalysis [2], gas adsorption and separation [3], biosensing and bioimaging [4], water purification [5], and drug delivery [6]. MOFs with partially coordinated metals, commonly known as coordinatively unsaturated metal sites (CUSs), can be obtained by removing the solvent via the activation step [7, 8]. MOF structures containing CUSs have great potential for drug adsorption. IRMOF-74 is a series of isoreticular MOF-74 that possess a similar topology that was initially synthesized by Yaghi et al. [9]. IRMOF-74 MOFs have become attractive for encapsulating drugs, since the magnesium (Mg) metal ion has low toxicity, and polycarboxylic linkers can be removed under physiological conditions [10].

The IRMOF-74 series comprises a variety of pore sizes such that each MOF can be employed for a specific amount of drug loading. For example, MOF-74-I demonstrated the lowest methotrexate (MTX) and 5-fluorouracil (5-FU) loading at 0.31 and 0.71 g.g<sup>-1</sup>, respectively, primarily due to the smallest pore size among the IRMOF-74 family members [11]. In contrast, IRMOF-74-XI showed 2.78 and 4.24 g.g<sup>-1</sup> for MTX and 5-FU storage, respectively. Preparing IRMOF-74s comprising CUSs has made them more efficient for drug adsorption. Fairen-Jimenez et al. elucidated that the

adsorption of ibuprofen (Ibu) inside MOF-74 pores was influenced by hydrogen bond (HB) interactions among polar hydrogen atoms in Ibu and the oxygen atoms surrounding Mg, and more importantly, the coordination bond between oxygen atoms in Ibu and Mg CUSs (O–Mg) [12].

The intrinsic tunability of pore size and pore wall surface in IRMOF-74-III (Figure 1-a) is achievable by incorporating functional groups on organic linkers via either pre-functionalization [13] or the post-synthetic modification (PSM) method [14]. For example, seven reactions based on the PSM method were carried out for sequential incorporating tripeptides on aminefunctionalized IRMOF-74-III [14]. Amine functionalization onto MOFs have been shown to improve drug adsorption [15–17]. Among the frequently investigated amine-functionalized MOFs, however, the effect of increasing the number of amine-functionalized organic linkers on drug adsorption has not been further investigated. Incorporating two amine groups on the phenyl ring in organic linkers as ortho, meta and para positions may potentially generate different dynamic and electronic conditions on the pore wall. Theoretical design and computational explorations are useful tools for a better understanding by reducing the cost of time and chemicals. Moreover, computational strategies provide a conceptual understanding physiochemical properties of organic linkers, desirable conformation of drug molecules on the MOF pore

surface, and host-guest interactions. These are crucial factors for rational functionalization, higher drug loading and controlled drug release.

In this work, we utilized computational methods to characterize a variety of amine-functionalized IRMOF-74-IIIs, hereafter referred to as IRM3 (Figure 1-b). Corresponding amine-functionalized IRM3 MOFs were then employed to encapsulate four non-steroidal anti-inflammatory drugs (NSAIDs), including aspirin (Asp), fenbufen (Fen), ibuprofen (Ibu) and naproxen (Nap)

(Figure 1-c). NSAIDs are consumed to ease the pain and inflammation by inhibiting the cyclooxygenase enzyme [18]. These drug compounds are frequently used by numerous researchers, as they are cheap and abundantly available in laboratories [19, 20]. Due to the hydrophobic property of NSAIDs, they are poorly-water soluble, which can result in erratic absorption and low bioavailability. Hence, encapsulating NSAID drug molecules within porous solid material such as MOFs is highly recommended to improve drug adsorption and delivery [21, 22].

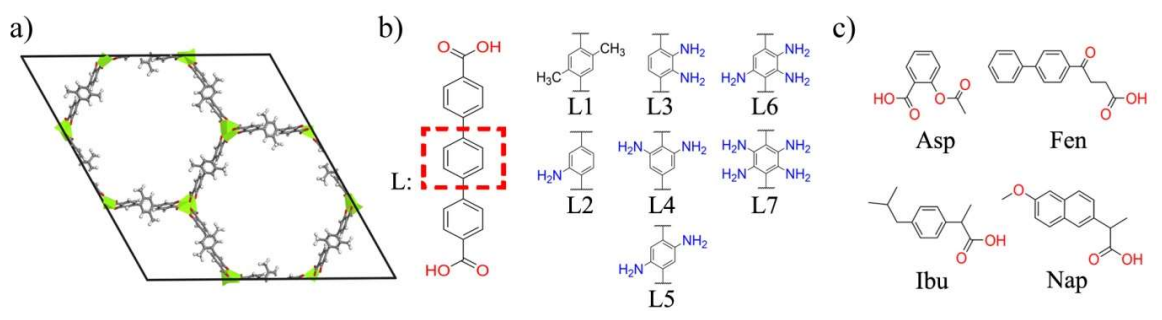


Figure 1. a) Unit cell of IRMOF-74-III, b) parent organic linker (L1) and the amine-functionalized organic linkers (L2-L7), and c) structure of NSAID drugs molecules

#### **Computational Details**

Geometry optimization of the organic linkers (L1-L7) was carried out using Gaussian 09 [23]. The structures were optimized at their ground state and gaseous phase. In order to characterize the organic linkers using an accurate level, DFT-B3LYP functional with a basis set of 6-31+G(d) was adopted. This level of computation generates highly accurate electronic properties. The corresponding basis set supports all atom types used in the frameworks (Mg, O, N, C, and H) and drug molecules (O, C, and H). Subsequently, the outputs allow us to analyze frontier molecular orbitals (FMOs), polarizability ( $\alpha$ ), topological polar surface area (TPSA) and dipole moments ( $\mu$ ) for organic linkers. At the same level of computation, single point energy calculation was carried out for the frameworks derived from the organic linkers to obtain the electrostatic potential (ESP) contours.

All amine-functionalized IRM3s were derived from the crystal structure of Mg-IRMOF-74-III available at the Cambridge Crystallographic Data Centre (CCDC), with

deposition code 841643 [9]. The unit cell was extended to 2×2×5, and the supercell model was situated in a vacuum box for docking calculation. Then, the center of the supercell was set for the grid box as 120×90×60 points in the three dimensions for the docking simulation. In addition, a grid spacing of 1.000 Å was set to cover the two central pores of the large frameworks. AutoDock version 4 and AutoDock Vina version 1.1.2 [24] were employed to implement the automated molecular docking calculation of drug molecules inside the MOFs. The Lamarckian genetic algorithm (LGA) combined with a grid-based energy evaluation method were applied to evaluate the grid maps. Gaussian 09 was utilized to calculate the atomic partial charges using the CHarges from ELectrostatic Potentials using a Grid-based (CHELPG) method [25] based on B3LYP/6-31+G(d) level.

The optimal pose of the drug molecules on the MOF surface was considered for natural bond orbital (NBO) analysis. The smaller cluster structures containing drug@MOF were separated from the docking results

and used for single point energy calculation at B3LYP/6-31+G(d) level. NBO version 3.1 [26], available in the Gaussian 09 package, was used for the energy calculation. The second-order perturbation theory from the NBO calculation was then used to identify the electron donor and acceptor between the NSAID drugs and the IRM3 frameworks.

#### **Results and Discussion**

Geometry optimization at level DFT-B3LYP/6-31+G(d) was implemented to interpret the physiochemical properties of the organic linkers (L1-L7). FMO analysis described the chemical reactivity of the proposed organic linkers. FMOs were divided into the highest

occupied molecular orbital (HOMO) and the lowest unoccupied molecular orbital (LUMO). HOMO orbitals were found to be distributed on the whole of the parent organic linker (L1). However, they were clearly localized on the middle phenyl ring when the methyl groups were replaced by amine groups (L2-L7) (Figure 2). The formation of HOMOs in all types of aminefunctionalized linkers followed the number and position of amine groups. Being localized HOMOs in the middle phenyl ring with different formations can be useful for donating electrons to the electrophilic sites in the drug molecules. On the other side, the formation of LUMO orbitals remained almost constant in all organic linkers (L1-L7).

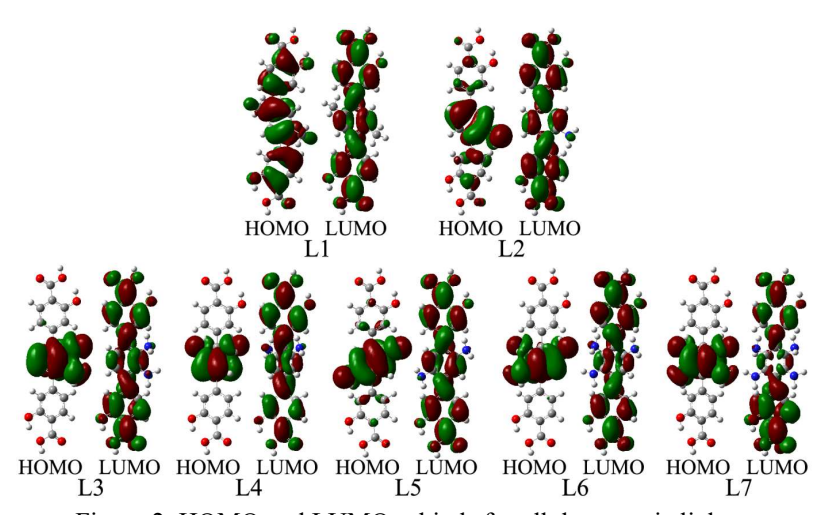


Figure 2. HOMO and LUMO orbitals for all the organic linkers

According to Table 1, the organic linkers demonstrated different values for the energy gap between the HOMO and LUMO orbitals (E<sub>HL</sub>), polarizability, TPSA and dipole moments. The values of E<sub>HL</sub> showed that increasing the substitution of the amine functional group on the organic linkers made them more kinetically stable. For example, the large value of E<sub>HL</sub> in L1 implies difficult electron transfer, whereas a small value of E<sub>HL</sub> in L7 indicates more facile electron transfer between HOMO and LUMO, as well as easier electrons donating to the electrophilic sites in the drug molecules. Incorporating the amine functional group generally caused the polarizability  $(\alpha)$  of the organic linkers to improve. The TPSA parameter determines the overall surface on all polar atoms within the molecular structure. The calculated TPSA confirmed the enhancement of the polar surface by increasing the amine group on linkers. Although the organic linker containing one amine group (L2) had the lowest polarizability (a), it produced a high amount of dipole moments ( $\mu$ ). Dipole moments play an important role in adsorption using MOFs. Srepusharawoot et al. studied the capability of four different metal-organic framework-525, namely, M-MOF-525 (M=Ti, V, Zr and Hf) for hydrogen adsorption using first-principles calculations [27]. The authors found that Zr- and Hf-MOF-525 were able to trap the hydrogen molecules on the surface due to stronger dipole moments. Also, zero values of dipole moment for L1 and L5 were obtained from para position of the functional groups, which means equal electron distributions on the middle phenyl ring.

Table 1	Physi	ochemic	al nro	nerties	for the	organic linkers
Table 1.	1 11 9 51	OCHCIIIC	ai pio	permes	IOI IIIC	organic inikcis

		1 1		
Compound	E <sub>HL</sub> (eV)	$\alpha$ (A <sup>3</sup> )	$TPSA(A^2)$	$\mu$ (D)
L1	4.41	46.24	115.1	0.00
L2	3.77	45.84	141.1	1.70
L3	3.58	46.52	167.1	1.29
L4	3.57	46.66	167.1	1.65
L5	3.14	47.59	167.1	0.00
L6	3.12	47.73	193.1	0.86
L7	2.76	48.24	219.1	0.64

In this report, the frameworks derived from the proposed organic linkers (L1-L7) are referred to as IRM3 (L1), IRM3-1 (L2), IRM3-20 (L3), IRM3-2m (L4), IRM3-p (L5), IRM3-3 (L6) and IRM3-4 (L7). The electrostatic potential (ESP) contours for all the frameworks are illustrated in Figure 3. The ESP contours revealed a highly distinguished pattern for each MOF's pore when the functionalized-amine groups were increased or placed in the *ortho*, *meta* or *para* positions. The conversion of the hexagonal ESP pattern in L1 to the trigonal ESP pattern for L2-L7 was attributed to the

different symmetry point group of the functional groups. The symmetry point group for the methyl and amine functional groups is  $C_{3\nu}$  and  $C_{2\nu}$ , respectively. Therefore, an R-3 symmetry was detected for the crystal structure of IRM3, whereas an R3 symmetry was observed for all amine-functionalized IRM3s. The EPS contours of the MOF crystals represented by red lines indicate negative potentials on the phenyl rings and the amine groups due to stronger electron distribution. This feature was amplified by increasing the amine groups on the linkers (the most for L7).

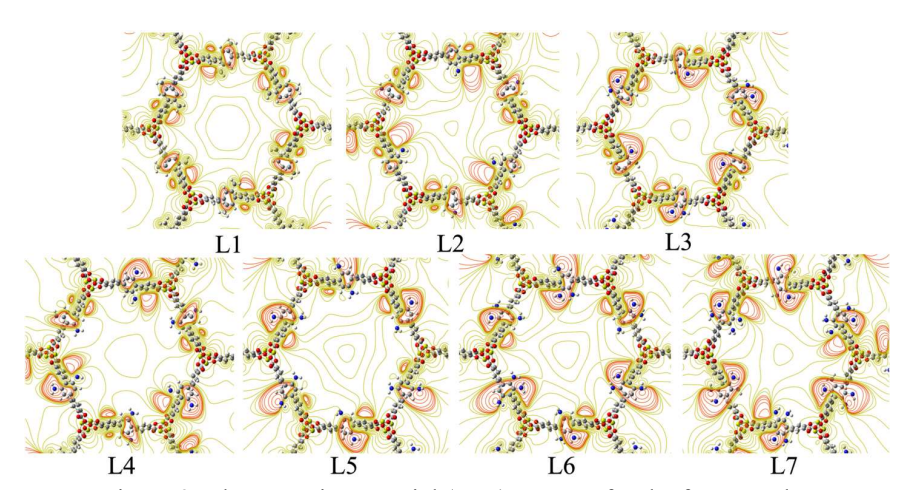


Figure 3. Electrostatic potential (ESP) contour for the frameworks

Overall, the DFT study of the organic linkers (L1-L7) and their corresponding frameworks demonstrated that HOMOs were localized where amine functional groups were incorporated in the middle phenyl ring. These changes were also illustrated by the ESP contour patterns. Middle phenyl rings had a higher electron density as the number of amine groups was increased. In addition, the values of polarizability  $(\alpha)$  and TPSA

demonstrated that increasing functional groups on IRM3 organic linker enhanced the polarity. It is expected that increasing the number of amine groups on IRM3 organic linkers would activate the MOF pore surface to trap more drug molecules by donating more electrons. All frameworks were further investigated for the adsorption of NSAID drug molecules by means of molecular docking simulation and NBO calculation to determine

## Borzehandani et al.: In Silico MODELLING OF DRUG ADSORPTION USING AMINE-FUNCTIONALIZED IRMOF-74-III METAL-ORGANIC FRAMEWORKS

the most favorable interaction site and the intensity of electron transmission, respectively. As depicted in Figure 4, all amine functionalized IRM3s produce different pockets (orange color) in the CUSs. This property could also be observed in the EPS contour. In

comparison, the tightest pocket in the CUSs tend to be in IRM3-2*o* and IRM3-4, whereas the largest pocket was in IRM3-2*m*. The distance between the amine groups on the linker clearly influence the size of pockets in the CUSs.

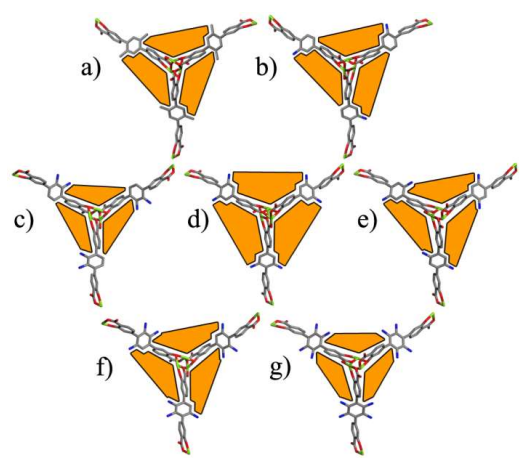


Figure 4. 2D schematic presentation of the pockets in CUSs for a) IRM3, b) IRM3-1, c) IRM3-2*o*, d) IRM3-2*m*, e) IRM3-2*p*, f) IRM3-3 and g) IRM3-4

Binding affinity can be defined as the degree of the binding of the drug molecules in the MOF pores [28]. Docking simulation using Autodock Vina produced nine modes of binding affinity (kcal mol-1) for each drug@MOFs complex system. The first (best) mode value was used to construct Figure 5. The variety of binding affinity values generated by each drug@MOF complex confirmed that the pockets on CUS sites had various spaces and morphologies. The highest binding affinity was produced by the Fen molecule, whereas the lowest binding affinity was exhibited by Asp. This result

could be attributed to their molecular size, as Fen and Asp have the largest and the smallest molecular size, respectively. The measured drug molecular size was shown as the order of Asp  $(10.6 \times 8.9 \text{ Å}) < \text{Ibu } (12.9 \times 7.8 \text{ Å}) < \text{Nap } (13.6 \times 7.9 \text{ Å}) < \text{Fen } (17.2 \times 7.5 \text{ Å})$ . Being the largest size of Fen led to the strongest fitting into the CUS pockets. In contrast, being the smallest size of Asp made it the least fitting. Moreover, Ibu and Nap docked into the CUS pockets and Asp due to a larger molecular size.

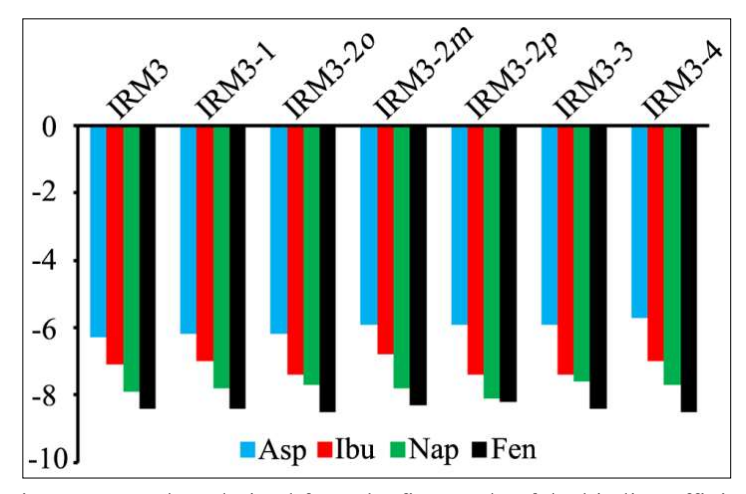


Figure 5. Bar chart derived from the first mode of the binding affinity

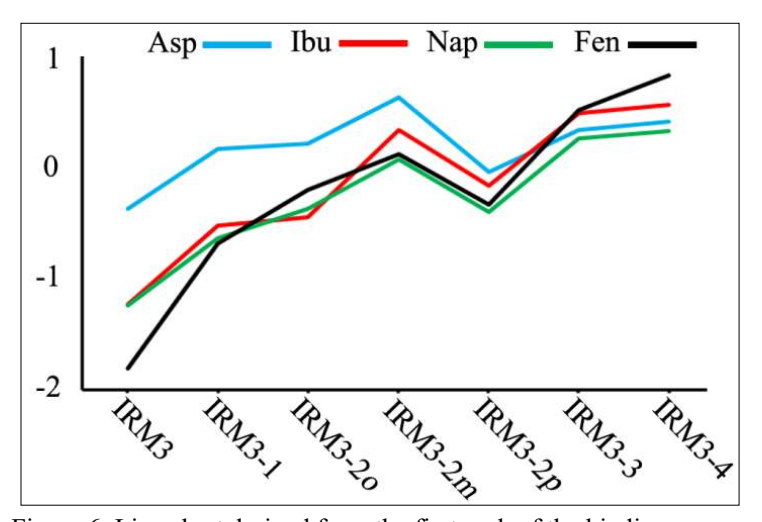


Figure 6. Line chart derived from the first rank of the binding energy

The highest rank of binding energy calculated by AutoDock is presented in Figure 6. The line chart shows a general upward trend for binding energies as the number of functionalized amine groups increase. These results suggest that the strength of the total interactions between the NSAID drug molecules and the frameworks was reduced. Drug molecules had a lower binding energy and stronger interactions when they were complexed in IRM3-2*p* compared to the other two isomers, IRM3-2*o* and IRM3-2*m*. Additionally, among the two isostructures, IRM3 and IRM3-2*p*, which differ only on the type of functional group, the positive charge of magnesium (Mg) (+1.3184) in IRM3 was reduced to +1.3003 in IRM3-2*p*. This change was governed by the inductive effect of the polar functional group such as the

amine group [29]. Thus, the binding energies produced by drug@IRM3 complex systems had the lowest values (the strongest interactions). In general, increasing amine groups on organic linkers reduced the strength of interactions in the drug@MOF complex systems.

Using MOF-1 and MOF-4, which have identical pore sizes, Zhang et al. observed reduced drug loading due to weaker interactions between Ibu and the pore surface [30]. It was shown that stronger interactions between the carboxyl group in Ibu and MOF-1 pore surface resulted in a two fold higher loading compared to MOF-4. In addition, the abundance of the secondary interactions such as hydrogen bond (HB), and electrostatic and hydrophobic interactions, play a crucial role in controlled drug release after drug loading [12, 31, 32].

Considering the matter of host-guest interactions, all types of interactions between the frameworks and the drug molecules were collected in Table 2. An analysis of the interactions indicated that the drug molecules mainly built interactions on the CUSs in IRM3, IRM3-1, IRM3-2m and IRM3-2p. On the other side, NSAID drugs were observed to have amine-based HB interactions when they were complexed in IRM3-2o, IRM3-3 and IRM3-4. The presence of two neighboring amine functional groups on the middle phenyl ring seemed dominant to CUS sites, since they provide large enough polar surfaces. Figure 7 shows an example of this behavior. The top three binding modes of Nap indicated that they were preferably placed on CUS sites in IRM3-2p. In contrast, they were concentrated on amine functional

groups in IRM3-3. By comparing the interaction distances in Table 2, we found that IRM3, IRM3-1, IRM3-2m and IRM3-2p generally provided abundant and strong interactions with drug molecules on CUSs. Some examples are metal-acceptor interactions (Mg<sub>framework</sub> ··· OC<sub>drug</sub>), oxygen-based HB interactions (O<sub>framework</sub> ··· HO<sub>drug</sub>), and plenty of hydrophobic ( $\pi$ -based) interactions. In contrast, drug molecules had amine-based HB interactions with IRM3-2o, particularly in IRM3-3 and IRM3-4. The results obtained indicate that the functionalizing of MOFs using two neighboring amine groups on organic linkers close to CUS sites would disrupt the capability of CUS for the adsorption of drug molecules.

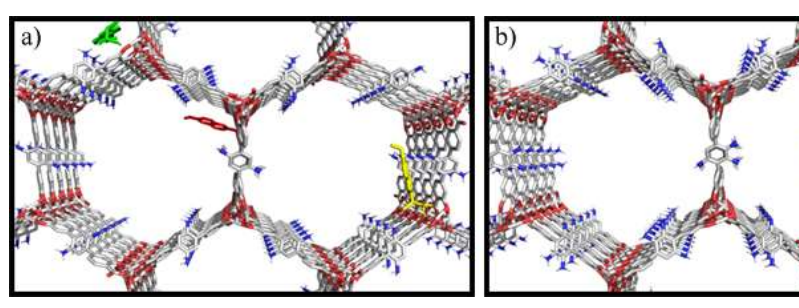


Figure 7. The top three binding modes of Nap in a) IRM3-2p and b) IRM3-3

Single point energy calculations allowed us to evaluate the electron transfer between the NSAID drug molecules and the frameworks using NBO analysis. The four highest NBO donor-acceptor interactions between the drug molecules and the frameworks are compiled in Tables 3 to 6. The atomic numbers of NSAID drug molecules are illustrated in Figure 8. The calculated stabilization energies ( $E_{ij}$ ) indicate that all the drug molecules transferred the most electrons when they were complexed with IRM3. Lone electron pair (LP) of oxygen atoms in the drug molecules and unfilled valence-shell nonbonding (LP\*) of Mg in the

frameworks played the primary role as the electron donor and the electron acceptor, respectively, in drug@IRM3, drug@IRM3-1, drug@IRM3-2o, drug@IRM3-2m, and drug@IRM3-2p. However, the NBO donor-acceptor interactions derived from drug@IRM3-3 and drug@IRM3-4 complex systems primarily involved the amine functional group, and the corresponding values of stabilization energies ( $E_{ij}$ ) were relatively poor. This evidence from NBO analysis confirmed that CUSs were the most favorable sites for stronger electron transfer and adsorption of the NSAIDs molecules.

Table 2. Interactions involved in all drug@MOF complex systems

-	Asp		Fer	1	Ib	<u> </u>	Na	Nap	
	Interaction Type	Distance (Å)	Interaction Type	Distance (Å)	Interaction Type	Distance (Å)	Interaction Type	Distance (Å)	
	$Mg \cdots OC_{Asp}$ $O \cdots OC_{Asp}$	1.74 2.56	O ··· OC <sub>Fen</sub> O ··· HO <sub>Fen</sub>	2.36 1.77	O ··· OC <sub>Ibu</sub> O ··· HO <sub>Ibu</sub>	2.38 1.98	O ··· OC <sub>Nap</sub> O ··· HO <sub>Nap</sub>	2.54 2.21	
13	π - π Stacked	3.72	Mg ··· CO <sub>Fen</sub>	1.77	Mg ··· CO <sub>Ibu</sub>	1.69	Mg ··· OC <sub>Nap</sub>	1.67	
IRM3	$\pi \cdots$ Alkyl	5.36	π - π T-shaped	5.13	π - π Stacked	4.29	$\pi \cdots HC_{Nap}$	3.40, 3.94	
Т	n may	3.30	$\pi$ ··· Alkyl	5.41, 4.61, 4.60	$\pi$ ··· Alkyl	4.36, 4.86, 5.07	$\pi$ ··· Alkyl	4.09, 4.55, 5.04, 5.38	
	NH · · · O <sub>Asp</sub>	1.74, 1.76	O ··· OC <sub>Fen</sub>	2.72	O · · · OC <sub>Ibu</sub>	2.76	$O \cdots HO_{Nap}$	1.95	
	$\pi$ - $\pi$ Stacked	3.95	$Mg\cdotsOC_{Fen}$	1.81	$O \cdots HO_{Ibu}$	1.85	$Mg\cdotsOC_{Nap}$	1.96	
IRM3-1			$\pi  \cdots  HC_{Fen}$	3.67	$Mg\cdotsOC_{Ibu}$	2.11	π - π Stacked	4.27, 5.31	
$\mathbf{z}$			π - $π$ Stacked	3.88	$\pi$ - $\pi$ T-shaped	5.07	$\pi$ - $\pi$ T-shaped	5.07, 5.15	
Ë			π - $π$ T-shaped	4.73, 5.44, 5.83	$\pi \cdots$ Alkyl	4.28, 4.62, 4.79, 5.22, 5.26, 5.36	$\pi \cdots Alkyl$	4.62	
	NH ··· O <sub>Asp</sub>	2.09	NH ··· HO <sub>Fen</sub>	2.19	NH · · · OC <sub>Ibu</sub>	2.44, 2.85	NH · · · OC <sub>Nap</sub>	1.95	
20	$O \cdots OC_{Asp}$	2.55	$O\cdotsOC_{Fen}$	2.48	$O \cdots HO_{Ibu}$	2.01	$O \cdots HO_{Nap}$	1.67	
<u>5</u>	$Mg\cdotsOC_{Asp}$	1.67	$Mg\cdotsOC_{Fen}$	1.72	$Mg\cdotsOC_{Ibu}$	1.82	$Mg\cdotsOC_{Nap}$	1.75	
IRM3-2 <i>o</i>	$\pi$ - $\pi$ Stacked	4.04	π - $π$ Stacked	3.92	$\pi$ · · · Anion	4.53	π - π Stacked	4.08, 4.15	
				5.46	π - $π$ Stacked	4.49			
					π···Alkyl	4.61, 4.86,			
_	NH · · · OC <sub>Asp</sub>	1.70	O ··· OC <sub>Fen</sub>	2.47, 2.74	O ··· OC <sub>Ibu</sub>	2.48, 2.99	O · · · OC <sub>Nap</sub>	2.64, 2.78	
.2m	$\pi$ - $\pi$ T-shaped	5.33	O ··· HO <sub>Fen</sub>	2.06	O ··· HO <sub>Ibu</sub>	2.04	NH · · · O <sub>Nap</sub>	2.18	
IRM3-2 <i>m</i>			$Mg \cdots OC_{Fen}$	1.75	Mg ··· OC <sub>Ibu</sub>	1.95	$Mg \cdots OH_{Nap}$	2.15	
ᢓ			$\pi$ ··· Cation	3.77, 4.13 3.43	Mg ··· OH <sub>Ibu</sub>	1.85	Mg ··· OC <sub>Nap</sub>	2.00	
_			π ··· Anion	3.43 3.96, 4.76	$\pi$ - $\pi$ Stacked	4.66	$\pi$ - $\pi$ Stacked	4.21, 4.53	
	O ··· OC <sub>Asp</sub>	2.69, 2.76	π - π Stacked Ο · · · OC <sub>Fen</sub>	2.81, 3.18	$\frac{\pi \cdots \text{Alkyl}}{\text{O} \cdots \text{OC}_{\text{Ibu}}}$	4.65 2.60	$\frac{\pi \cdots \text{Alkyl}}{\text{NH} \cdots \text{O}_{\text{Nap}}}$	2.16	
	NH ··· OC <sub>Asp</sub>	1.95	O ··· HO <sub>Fen</sub>	2.08	O ··· HO <sub>Ibu</sub>	1.94	$O \cdots OC_{Nap}$	2.36, 3.01	
2p	Mg ··· OC <sub>Asp</sub>	1.90	Mg ··· OC <sub>Fen</sub>	1.91	Mg ··· OC <sub>Ibu</sub>	1.70	O ··· HO <sub>Nap</sub>	1.90	
IRM3-2 <i>p</i>	π - π Stacked	3.88	$\pi$ ··· Cation	4.07	$\pi$ - $\pi$ T-shaped	5.61	$Mg \cdots OC_{Nap}$	1.91	
Z			$\pi$ · · · Anion	3.83	1		$\pi$ ··· Cation	4.91	
Ι							π - π Stacked	4.08, 4.23	
							π··· Alkyl	4.57, 5.24	
6	NH · · · O <sub>Asp</sub>	1.75, 1.84	NH · · · O <sub>Fen</sub>	1.74	NH ··· O <sub>Ibu</sub>	1.72, 1.75	NH · · · O <sub>Nap</sub>	1.74, 1.84	
IRM3-3			$\pi$ - $\pi$ Stacked	3.64, 5.62					
			π - π T-shaped	5.24					
IRM3-4	NH ··· O <sub>Asp</sub>	1.90, 2.03	NH ··· O <sub>Fen</sub>	1.62, 1.63	NH ··· O <sub>Ibu</sub>	1.76, 1.87	NH ··· O <sub>Nap</sub>	1.62, 1.63	

<sup>\*</sup> Atom symbol without subscript belongs to the framework

a) 
$$H_3$$
  $H_4$  b)  $H_{15} H_{14} H_{13}$   $C_{12} H_7$   $H_6 H_5 H_4$   $H_{12} C_{11}$   $C_{6} = C_{5}$   $C_{3} - H_{3}$   $C_{10} - C_{7}$   $C_{4} - C_{2} - H_{2}$   $C_{11} C_{6} = C_{5}$   $C_{3} - H_{3}$   $C_{10} - C_{7}$   $C_{4} - C_{2} - H_{2}$   $C_{11} C_{6} = C_{5} C_{5} C_{3} - H_{3}$   $C_{10} - C_{7} C_{7} C_{4} - C_{2} - H_{2}$   $C_{11} C_{8} C_{8} - C_{9} C_{1} - O_{1}$   $C_{8} - C_{9} C_{1} - O_{1}$   $C_{8} - C_{9} C_{1} - O_{1}$   $C_{11} - C_{8} C_{12} C_{7} - C_{6}$   $C_{11} - C_{12} C_{12} C_{12} C_{12}$   $C_{12} - C_{14} C_{11} - C_{8} C_{9} C_{10} C_{12} C_{12} C_{12} C_{12} C_{12}$   $C_{12} - C_{13} C_{12} C_{12}$ 

Figure 8. Atomic numbers for a) Asp, b) Ibu, c) Fen and d) Nap used in Tables 3-6

Table 3. The highest four NBO donor-acceptor interactions for Asp@MOF complex systems

Asp@MOFs	Donor (i) → Acceptor (j)	E <sub>ij</sub> (kcal/mol)	Donor (i) → Acceptor (j)	Eij (kcal/mol)
Asp@IRM3	1: LP (2) $O_4 \to LP^*$ (3) Mg	29.53	2: LP (2) $O_4 \rightarrow LP^*$ (2) Mg	9.00
	3: BD (1) $O_4 - H_1 \rightarrow LP^*$ (3) N	Mg 8.19	4: LP (2) $O_4 \rightarrow LP^*$ (1) Mg	6.64
Asp@IRM3-1	1: LP (2) $O_2 \rightarrow LP^*$ (1) Mg	16.19	2: LP (2) $O_4 \rightarrow LP^*$ (1) Mg	11.56
	3: LP (2) $O_2 \to LP^*$ (3) Mg	11.21	4: BD (1) $C_1$ - $O_2 \rightarrow LP^*$ (1) Mg	4.52
Asp@IRM3-2o	1: LP (1) $O_3 \to LP^*$ (3) Mg	16.24	2: LP (2) $O_1 \rightarrow LP^*$ (2) Mg	12.05
	3: LP (1) $O_3 \to BD^*$ (1) N-H	5.36	4: LP (1) $O_2 \to BD^*$ (1) N-H	4.28
Asp@IRM3-2m	1: LP (2) $O_2 \to LP^*$ (1) Mg	14.83	2: LP (2) $O_2 \rightarrow LP^*$ (3) Mg	13.77
	3: LP (2) $O_4 \rightarrow LP^*$ (1) Mg	10.26	4: LP (1) $O_4 \rightarrow LP^*$ (1) Mg	4.88
Asp@IRM3-2p	1: LP (1) $O_4 \rightarrow LP^*$ (3) Mg	16.26	2: LP (2) $O_2 \rightarrow LP^*$ (1) Mg	14.31
	3: LP (1) O $\rightarrow$ BD* (1) O <sub>4</sub> -H <sub>1</sub>	11.04	4: LP (2) $O_2 \to LP^*$ (3) Mg	10.60
Asp@IRM3-3	1: LP (1) $O_3 \to BD^*$ (1) N-H	5.58	2: LP (1) $O_4 \rightarrow BD$ (1) N-H	4.57
	3: LP (1) $O_4 \to BD^*$ (2) N-H	3.24	4: BD (1) $C_6$ -H <sub>5</sub> $\rightarrow$ BD* (1) N-H	0.61
Asp@IRM3-4	1: LP (1) N $\rightarrow$ BD* (1) O <sub>4</sub> -H <sub>1</sub>	6.02	2: LP (2) $O_4 \to BD^*$ (1) N-H	5.42
	3: BD (1) O <sub>4</sub> -H <sub>1</sub> $\rightarrow$ BD* (1) N-	-Н 4.47	4: LP (1) $O_4 \rightarrow BD$ (1) N-H	3.56

<sup>\*</sup> Atom symbol without subscript is belong to the framework

Table 4. The highest four NBO donor-acceptor interactions for Fen@MOF complex systems

Fen@MOFs	Donor (i) → Acceptor (j)	E <sub>ij</sub> (kcal/mol)	Donor (i) → Acceptor (j)	E <sub>ij</sub> (kcal/mol)
Fen@IRM3	1: LP (1) $O_1 \to LP^*$ (3) Mg	18.63	2: LP (1) $O_1 \to LP^*$ (2) Mg	15.54
	3: BD (1) $O_1$ - $H_1 \to LP^*$ (2) Mg	11.57	4: LP* (2) Mg $\rightarrow$ BD* (1) O <sub>1</sub> -H <sub>1</sub>	8.91
Fen@IRM3-1	1: LP (2) $O_1 \to LP^*$ (2) Mg	5.90	2: BD (2) $C_{16}$ - $C_{15} \rightarrow LP^*$ (4) Mg	4.51
	3: BD (1) $C_{16}$ - $H_{14} \rightarrow LP^*$ (2) Mg	3.66	4: LP (1) $O_1 \to LP^*$ (2) Mg	3.52
Fen@IRM3-2o	1: LP (2) $O_1 \to LP^*$ (3) Mg	29.41	2: BD (1) $O_2 \to LP^*$ (2) Mg	8.66
	3: LP (1) $O_1 \to BD^*$ (1) N-H	3.07	4: LP (1) $O_3 \to BD^*$ (1) N-H	2.87
Fen@IRM3-2m	1: BD (2) $C_{16}$ - $C_{15} \rightarrow LP^*$ (4) Mg	4.02	2: LP (2) $O_1 \to LP^*$ (2) Mg	3.57
	3: BD (1) $C_{16}$ - $H_{14} \rightarrow LP^*$ (2) Mg	3.25	4: BD (2) $C_{16}$ - $C_{15} \rightarrow LP^*$ (3) Mg	2.90
Fen@IRM3-2p	1: LP (1) $O_1 \to LP^*$ (2) Mg	4.00	2: BD (2) $C_{13}$ - $C_{12} \rightarrow LP^*$ (4) Mg	3.59
	3: BD (1) $C_{12}$ - $H_{10} \rightarrow LP^*$ (2) Mg	3.59	4: LP (2) $O_1 \to LP^*$ (2) Mg	3.37
Fen@IRM3-3	1: LP (1) $O_1 \to BD^*$ (1) N-H	6.44	2: LP (2) $O_3 \to BD^*$ (1) N-H	5.07
	3: BD (1) $C_{10}$ - $H_9 \rightarrow BD^*$ (1) N-H	3.87	4: LP (1) $O_1 \rightarrow BD$ (2) N-H	3.17
Fen@IRM3-4	1: LP (2) $O_3 \to BD^*$ (1) N-H	4.81	2: LP* (3) N-H $\rightarrow$ BD* (1) O <sub>1</sub> -H <sub>1</sub>	4.52
	3: LP (1) $O_1 \to BD^*$ (1) N-H	3.29	4: LP (1) $O_1 \to BD^*$ (2) N-H	3.05

<sup>\*</sup> Atom symbol without subscript is belong to the framework

Table 5. The highest four NBO donor-acceptor interactions for Ibu@MOF complex systems

Ibu@MOFs	Donor (i) → Acceptor (j)	$E_{ij}$	Donor (i) → Acceptor (j)	$E_{ij}$
		(kcal/mol)		(kcal/mol)
Ibu@IRM3	1: LP (1) $O_1 \to LP^*$ (3) Mg	26.77	2: LP (2) $O_1 \to LP^*$ (2) Mg	13.37
	3: BD (1) $O_1$ - $H_1 \to LP^*$ (3) Mg	9.29	4: BD (1) $O_1$ - $H_1 \to LP^*$ (2) Mg	6.47
Ibu@IRM3-1	1: LP (1) $O_1 \to LP^*$ (2) Mg	14.37	2: LP (2) $O_1 \to LP^*$ (4) Mg	12.56
	3: LP (2) $O_1 \rightarrow LP^*$ (2) Mg	11.25	4: BD (1) $O_1$ - $H_1 \rightarrow LP^*$ (3) Mg	9.91
Ibu@IRM3-2o	1: LP (2) $O_1 \to LP^*$ (3) Mg	17.32	2: LP (1) $O_1 \rightarrow LP^*$ (2) Mg	12.58
	3: LP (1) $O_1 \rightarrow BD$ (1) N-H	5.10	4: LP (1) $O_3 \to BD^*$ (2) N-H	3.76
Ibu@IRM3-2 <i>m</i>	1: LP (1) $O_1 \to LP^*$ (4) Mg	16.26	2: LP (1) $O_1 \to LP^*$ (2) Mg	11.36
	3: BD (1) $O_1$ - $H_1 \to LP^*$ (3) Mg	9.05	4: LP (2) $O_1 \rightarrow LP^*$ (2) Mg	8.22
Ibu@IRM3-2p	1: LP (2) $O_1 \to LP^*$ (2) Mg	13.95	2: BD (1) $C_{13}$ - $H_{18} \rightarrow LP^*$ (4) Mg	8.36
	3: BD (1) $C_9$ - $H_9 \rightarrow LP^*$ (4) Mg	6.04	4: LP (1) O $\rightarrow$ BD* (1) C <sub>11</sub> -H <sub>12</sub>	4.55
Ibu@IRM3-3	1: LP (1) O $\rightarrow$ BD* (1) C <sub>2</sub> -H <sub>2</sub>	5.34	2: BD (2) $C_1$ - $O_2 \to BD^*$ (1) N-H	4.53
	3: LP (1) $O_1 \rightarrow BD$ (1) N-H	4.19	4: LP (1) O $\rightarrow$ BD (2) C <sub>2</sub> -H <sub>2</sub>	3.04
Ibu@IRM3-4	1: LP (3) O $\rightarrow$ BD* (1) O <sub>1</sub> -H <sub>1</sub>	4.56	2: LP (1) $O_1 \rightarrow BD^*$ (1) N-H	3.68
	3: LP (1) $O_1 \rightarrow BD$ (1) N-H	3.16	4: BD (1) N-H $\rightarrow$ BD* (1) C <sub>8</sub> -H <sub>9</sub>	2.88

<sup>\*</sup> Atom symbol without subscript is belong to the framework

Table 6. The highest four NBO	donor-acceptor interactions for	or Nap@MOF complex systems

Nap@MOFs	Donor (i) → Acceptor (j)	$E_{ij}$	Donor (i) → Acceptor (j)	E <sub>ij</sub>
		(kcal/mol)	Donor (i) Areceptor (j)	(kcal/mol)
Nap@IRM3	1: LP* (4) Mg $\rightarrow$ BD* (1) O <sub>1</sub> -H <sub>1</sub>	15.55	2: LP (2) $O_1 \rightarrow LP^*$ (2) Mg	14.67
	3: BD (1) $O_1$ - $H_1 \to LP^*$ (4) Mg	14.61	4: LP (1) $O_1 \to LP^*$ (3) Mg	12.00
Nap@IRM3-1	1: LP (1) $O_1 \rightarrow LP^*$ (3) Mg	12.19	2: BD (1) $O_1$ - $H_1 \to LP^*$ (4) Mg	8.86
	3: LP (1) $O_1 \rightarrow LP^*$ (4) Mg	8.07	4: BD (1) $O_1$ - $H_1 \rightarrow LP^*$ (3) Mg	6.66
Nap@IRM3-2o	1: LP (2) $O_2 \rightarrow LP^*$ (3) Mg	13.75	2: BD (1) $O_2 \rightarrow LP^*$ (3) Mg	12.24
	3: BD (1) $O_1 \to LP^*$ (3) Mg	6.21	4: LP (1) $O_1 \rightarrow BD$ (1) N-H	4.10
Nap@IRM3-2m	1: LP (1) $O_1 \to LP^*$ (3) Mg	14.03	2: BD (1) $O_1$ - $H_1 \to LP^*$ (3) Mg	13.04
	3: LP (2) $O_1 \rightarrow LP^*$ (4) Mg	10.70	4: BD (1) $C_1$ - $O_1 \rightarrow LP^*$ (3) Mg	7.41
Nap@IRM3-2p	1: LP (1) $O_1 \to LP^*$ (3) Mg	13.87	2: BD (1) $O_1$ - $H_1 \to LP^*$ (3) Mg	9.70
	3: BD (1) $C_1$ - $O_1 \rightarrow LP^*$ (3) Mg	7.30	4: BD (1) $O_1$ - $H_1 \to LP^*$ (4) Mg	5.82
Nap@IRM3-3	1: BD (1) $C_{10}$ - $H_9 \rightarrow BD^*$ (1) N-H	5.55	2: BD (1) N-H $\rightarrow$ BD* (1) C <sub>10</sub> -H <sub>9</sub>	5.07
	3: LP (1) $O_2 \to BD^*$ (1) N-H	4.05	4: BD (1) $C_{10}$ -H <sub>9</sub> $\rightarrow$ BD* (1) N-H	3.91
Nap@IRM3-4	1: LP (1) N $\rightarrow$ BD* (1) C <sub>3</sub> -H <sub>5</sub>	4.66	2: LP (1) N $\rightarrow$ BD* (1) C <sub>3</sub> -H <sub>5</sub>	3.87
	3: BD (1) $C_{10}$ -H <sub>9</sub> $\rightarrow$ BD* (1) N-H	3.68	4: LP (1) $O_1 \rightarrow BD$ (1) N-H	2.21

<sup>\*</sup> Atom symbol without subscript is belong to the framework

#### Conclusion

In this computational work, a set of aminefunctionalized IRM3 was derived from the parent structure (IRMOF-74-III). Initially, all organic linkers (L1-L7) were characterized at the DFT level. The results indicated that the increase of the amine group on organic linkers extended the polarity of the MOF pore surface and decreased the values of  $E_{\text{HL}}$ . The reduced  $E_{\text{HL}}$  in the MOFs containing more amine groups indicate their capability to donate electrons to drug molecules during binding. This was corroborated by the evaluation of framework-drug interactions and NBO analysis. NSAID drug molecules were found to prefer accommodating on CUS sites, which resulted in a variety of frameworkdrug interactions and a stronger electron transfer. In this set of drug@MOF complex systems, NBO analysis revealed that electron transfer from lone pair of electrons on oxygen atoms in the drugs to magnesium CUSs had the highest energy stabilization. Meanwhile, drug molecules were found more on organic linkers, making amine-based HB interactions when two neighboring amine groups were present such as in IRM3-20, IRM3-3 and IRM3-4 MOFs. In addition, it was found that larger NSAID drug molecules had better fit into the CUS sites in the order of Fen > Nap > Ibu >

Asp. Our results provide valuable insights on functionalizing MOF containing CUS sites with amine groups to improve drug encapsulation.

#### Acknowledgements

The authors would like to acknowledge the Ministry of Education (MOE) Malaysia. This research is supported by the Ministry of Education (MOE) Malaysia through Fundamental Research Grant Scheme (FRGS/1/2020/STG04/UPM/02/9).

#### References

- Kitagawa, S. (2014). Metal-organic frameworks (MOFs). Chemical Society Reviews, 43(16): 5415-5418.
- Zhu, L., Liu, X. Q., Jiang, H. L. and Sun, L. B. (2017). Metal–organic frameworks for heterogeneous basic catalysis. *Chemical reviews*, 117(12): 8129-8176.
- 3. Li, J. R., Ma, Y., McCarthy, M. C., Sculley, J., Yu, J., Jeong, H. K. and Zhou, H. C. (2011). Carbon dioxide capture-related gas adsorption and separation in metal-organic frameworks. *Coordination Chemistry Reviews*, 255(15-16): 1791-1823.

- 4. Wang, H. S. (2017). Metal—organic frameworks for biosensing and bioimaging applications. *Coordination Chemistry Reviews*, 349: 139-155.
- Feng, M., Zhang, P., Zhou, H. C. and Sharma, V. K. (2018). Water-stable metal-organic frameworks for aqueous removal of heavy metals and radionuclides: A review. *Chemosphere*, 209: 783-800.
- Lázaro, I. A. and Forgan, R. S. (2019). Application of zirconium MOFs in drug delivery and biomedicine. *Coordination chemistry reviews*, 380: 230-259.
- Zhang, X., Wang, J., Dong, X. X. and Lv, Y. K. (2020). Functionalized metal-organic frameworks for photocatalytic degradation of organic pollutants in environment. *Chemosphere*, 242: 125144.
- Zheng, X., Zhang, L., Fan, Z., Cao, Y., Shen, L., Au, C. and Jiang, L. (2019). Enhanced catalytic activity over MIL-100 (Fe) with coordinatively unsaturated Fe<sup>2+</sup>/Fe<sup>3+</sup> sites for selective oxidation of H<sub>2</sub>S to sulfur. *Chemical Engineering Journal*, 374: 793-801.
- Deng, H., Grunder, S., Cordova, K. E., Valente, C., Furukawa, H., Hmadeh, M. and Yaghi, O. M. (2012). Large-pore apertures in a series of metalorganic frameworks. *Science*, 336(6084): 1018-1023.
- Kotzabasaki, M., Galdadas, I., Tylianakis, E., Klontzas, E., Cournia, Z. and Froudakis, G. E. (2017). Multiscale simulations reveal IRMOF-74-III as a potent drug carrier for gemcitabine delivery. *Journal of Materials Chemistry B*, 5(18): 3277-3282.
- Erucar, I. and Keskin, S. (2017). Computational investigation of metal organic frameworks for storage and delivery of anticancer drugs. *Journal of Materials Chemistry B*, 5(35): 7342-7351.
- 12. Bernini, M. C., Fairen-Jimenez, D., Pasinetti, M., Ramirez-Pastor, A. J. and Snurr, R. Q. (2014). Screening of bio-compatible metal-organic frameworks as potential drug carriers using Monte Carlo simulations. *Journal of Materials Chemistry B*, 2(7): 766-774.
- 13. Fracaroli, A. M., Furukawa, H., Suzuki, M., Dodd, M., Okajima, S., Gándara, F. and Yaghi, O. M.

- (2014). Metal—organic frameworks with precisely designed interior for carbon dioxide capture in the presence of water. *Journal of the American Chemical Society*, 136(25): 8863-8866.
- Fracaroli, A. M., Siman, P., Nagib, D. A., Suzuki, M., Furukawa, H., Toste, F. D. and Yaghi, O. M. (2016). Seven post-synthetic covalent reactions in tandem leading to enzyme-like complexity within metal—organic framework crystals. *Journal of the American Chemical Society*, 138(27): 8352-8355.
- Van Tran, T., Nguyen, D. T. C., Le, H. T. N., Vo, D. V. N., Doan, V. D., Dinh, V. P. and Bach, L. G. (2019). Amino-functionalized MIL-88B (Fe)-based porous carbon for enhanced adsorption toward ciprofloxacin pharmaceutical from aquatic solutions. *Comptes Rendus Chimie*, 22(11-12): 804-812.
- Xu, X. Y. and Yan, B. (2016). Selective detection and controlled release of Aspirin over fluorescent amino-functionalized metal—organic framework in aqueous solution. Sensors and Actuators B: Chemical, 230: 463-469.
- 17. Almáši, M., Zeleňák, V., Palotai, P., Beňová, E. and Zeleňáková, A. (2018). Metal-organic framework MIL-101 (Fe)-NH2 functionalized with different long-chain polyamines as drug delivery system. *Inorganic Chemistry Communications*, 93: 115-120.
- Smith, S. R., Deshpande, B. R., Collins, J. E., Katz, J. N. and Losina, E. (2016). Comparative pain reduction of oral non-steroidal anti-inflammatory drugs and opioids for knee osteoarthritis: systematic analytic review. *Osteoarthritis and cartilage*, 24(6): 962-972.
- 19. Juère, E., Florek, J., Bouchoucha, M., Jambhrunkar, S., Wong, K. Y., Popat, A. and Kleitz, F. (2017). In vitro dissolution, cellular membrane permeability, and anti-inflammatory response of resveratrolencapsulated mesoporous silica nanoparticles. *Molecular Pharmaceutics*, 14(12): 4431-4441.
- Koç, F. E. and Şenel, M. (2013). Solubility enhancement of non-steroidal anti-inflammatory drugs (NSAIDs) using polypolypropylene oxide core PAMAM dendrimers. *International journal of* pharmaceutics, 451(1-2): 18-22.

## Borzehandani et al.: In Silico MODELLING OF DRUG ADSORPTION USING AMINE-FUNCTIONALIZED IRMOF-74-III METAL-ORGANIC FRAMEWORKS

- Rivas, C. J. M., Tarhini, M., Badri, W., Miladi, K., Greige-Gerges, H., Nazari, Q. A. and Elaissari, A. (2017). Nanoprecipitation process: From encapsulation to drug delivery. *International journal of pharmaceutics*, 532(1): 66-81.
- Shishir, M. R. I., Xie, L., Sun, C., Zheng, X. and Chen, W. (2018). Advances in micro and nanoencapsulation of bioactive compounds using biopolymer and lipid-based transporters. *Trends in Food Science & Technology*, 78: 34-60.
- 23. Frisch, M. J., Trucks, G. W., Schlegel, H. B., Scuseria, G. E., Robb, M. A., Cheeseman, J. R. and Fox, D. J. (2009). Gaussian 09 Program; Gaussian, Inc. *Wallingford*, *CT*.
- 24. Trott, O. and Olson, A. J. (2010). AutoDock Vina: improving the speed and accuracy of docking with a new scoring function, efficient optimization, and multithreading. *Journal of Computational Chemistry*, 31(2): 455-461.
- Liu, J. Q., Li, X. F., Gu, C. Y., da Silva, J. C., Barros, A. L., Alves-Jr, S. and Soares, T. A. (2015). A combined experimental and computational study of novel nanocage-based metal-organic frameworks for drug delivery. *Dalton Transactions*, 44(44): 19370-19382.
- 26. Weinhold, F. and Glendening, E. D. (2001). NBO 5.0 program manual: natural bond orbital analysis programs. *Theoretical Chemistry Institute and Department of Chemistry, University of Wisconsin, Madison, WI*, 53706.
- 27. Suksaengrat, P., Amornkitbamrung, V. and

- Srepusharawoot, P. (2020). Enhancements of hydrogen adsorption energy in M-MOF-525 (M= Ti, V, Zr and Hf): A DFT study. *Chinese Journal of Physics*, 64: 326-332.
- Rodrigues, M. O., de Paula, M. V., Wanderley, K. A., Vasconcelos, I. B., Alves Jr, S. and Soares, T. A. (2012). Metal organic frameworks for drug delivery and environmental remediation: A molecular docking approach. *International Journal of Quantum Chemistry*, 112(20): 3346-3355.
- 29. Pham, T., Forrest, K. A., Nugent, P., Belmabkhout, Y., Luebke, R., Eddaoudi, M. and Space, B. (2013). Understanding hydrogen sorption in a metalorganic framework with open-metal sites and amide functional groups. *The Journal of Physical Chemistry C*, 117(18): 9340-9354.
- 30. Sun, K., Li, L., Yu, X., Liu, L., Meng, Q., Wang, F. and Zhang, R. (2017). Functionalization of mixed ligand metal-organic frameworks as the transport vehicles for drugs. *Journal of colloid and interface science*, 486: 128-135.
- 31. Hai, T., Wan, X., Yu, D. G., Wang, K., Yang, Y. and Liu, Z. P. (2019). Electrospun lipid-coated medicated nanocomposites for an improved drug sustained-release profile. *Materials & Design*, 162: 70-79.
- 32. Hate, S. S., Reutzel-Edens, S. M. and Taylor, L. S. (2020). Influence of drug-silica electrostatic interactions on drug release from mesoporous silica-based oral delivery systems. *Molecular Pharmaceutics*, 17(9): 3435-3446.